Observation of a Reversible Thermotropic Order–Order Transition in a Diblock Copolymer

Damian A. Hajduk and Sol M. Gruner*

Department of Physics, Princeton University, Princeton, New Jersey 08544

Pratima Rangarajan and Richard A. Register

Department of Chemical Engineering, Princeton University, Princeton, New Jersey 08544

Lewis J. Fetters

Exxon Research and Engineering Company, Corporate Research Science Lab, Clinton Township, Annandale, New Jersey 08801

Christian Honeker, Ramon J. Albalak,† and Edwin L. Thomas

Department of Materials Science and Engineering, Massachusetts Institute of Technology, Cambridge, Massachusetts 02139

Received July 28, 1993; Revised Manuscript Received October 9, 1993®

ABSTRACT: We report the observation of a reversible thermotropic transition between the lamellar and cylindrical morphologies in a polystyrene–poly(ethene-*co*-butene) diblock copolymer. The nature of the intermediate structures which form as the transition progresses has been examined using two-dimensional small-angle X-ray scattering (SAXS) and transmission electron microscopy (TEM). Results show that the transformation from the lamellar to the cylindrical morphology proceeds in two steps. Initially, fluctuations along the interface joining the components of the copolymer grow in amplitude until the lamella transforms into a sheet of evenly spaced cylinders; cylinders which form in adjacent lamellae are usually in poor register with one another. This intermediate structure subsequently anneals into the hexagonal packing of cylinders characteristic of the cylindrical morphology. The reverse transition from cylinders to lamellae proceeds without producing any intermediate signature detectable by SAXS.

Introduction

The microphase structure of a diblock copolymer melt is determined by several physical parameters.[1] Theory suggests that a given polymer will adopt the morphology which minimizes the interfacial area per chain junction point while maximizing the entropy of both blocks. These factors depend, in turn, on the geometry of the microphase, the relative lengths (or volume fractions) of the two blocks, the relative incompatibility of the two blocks, and differences in the statistical segment lengths. Symmetric polymers in the strong segregation limit, in which the minority (A) and majority (B) blocks are of roughly equal segmental volume, tend to form alternating lamellae of A and B. As the volume fraction of A decreases, a three-dimensional bicontinuous network of A and B domains is observed (the ordered bicontinuous double diamond structure, or OBDD). Next come hexagonally packed cylinders of A in a matrix of B and then spherical domains of A arranged on a body-centered-cubic lattice in a matrix of B.

Although the equilibrium morphologies in the strong segregation limit are themselves well characterized, the detailed processes by which they form are relatively unexplored. A block copolymer at a sufficiently high temperature or in a dilute solution exists in a homogeneous disordered state. In the former case, the segment–segment interaction parameter has been reduced by temperature; in the latter case, the solvent molecules screen out the energetically unfavorable contacts between A and B segments. As the temperature is lowered or as solvent leaves the system, the strength of segmental interactions increases and, at some point, phase separation of the A and B blocks occurs. Microphase-separated structures with long-range order may now form, and the system may appear to reach an equilibrium configuration.

Most studies of microphase ordering in neat block copolymer systems have focused on the kinetics of the order-disorder transition (ODT) which occurs in the weak segregation limit.[3–6] Studies have used low molecular weight polymers, polymer solutions, or polymers with an inherently small segmental interaction parameter to reach the weak segregation limit and avoid thermal degradation problems. Using short chains or solutions also accelerates the kinetics of the transition. Microphase transitions between different ordered morphologies in the weak segregation regime have been identified by small-angle neutron scattering (SANS) and rheological measurements.[1,2,7]

Considerable research has been devoted to the behavior of block copolymers in the presence of selective and nonselective solvents; by choosing an appropriate combination of polymers and solvent, one may examine behavior in either the weak, intermediate,[8,9] or strong segregation regimes. Good reviews of early work are given by Sadron and Gallot;[10,11] more recent work has been performed by Shibayama *et al.*[12–14] and Sakurai *et al.*[15] The latter authors have reported reversible transitions between ordered morphologies for block copolymers in the presence of solvent. It has long been recognized that the morphology observed in a bulk film may depend on the solvent from which the film is cast;[16] selective swelling of one block of the polymer by a preferential solvent may result in a different bulk morphology than that observed when a nonpreferential solvent is used. Such nonequilibrium morphologies are metastable below the glass

* To whom correspondence should be addressed.
† Current address: Israel Plastics and Rubber Center, Technion City, Haifa 32000, Israel.
® Abstract published in *Advance ACS Abstracts*, December 15, 1993.

0024-9297/94/2227-0490$04.50/0

transition temperatures of one or both blocks in the polymer; annealing the film at elevated temperatures should in principle return the sample to the equilibrium morphology. Transitions of this sort have been observed with SAXS and TEM;[17-19] these studies provide much of what little is known about order–order transitions in the intermediate and strong segregation regimes.

For our purposes, such studies have a serious drawback. Typical nonequilibrium-to-equilibrium studies begin by forcing the system so far from equilibrium that it is unclear that the insights gained by studying the resulting relaxation behavior (where the gradient in free energy returning the polymer to the equilibrium state is initially very large) may be successfully applied to microdomain formation under less extreme conditions. More applicable information might be obtained by examining an order–order transition between two equilibrium morphologies in a bulk film, such as has been done recently by Sakurai *et al.*[20] for a transition between a cylindrical morphology and a body-centered-cubic arrangement of spheres. When examining such transitions, several considerations must be kept in mind. The free energy barriers separating different microstructures may be quite large, implying that once a polymer has adopted a particular morphology, a transition to another morphology may proceed extremely slowly. Extreme conditions, such as high-temperature annealing or significant mechanical deformation, may be needed to lift the system over these free energy barriers. When using high molecular weight materials, such transitions, though energetically favorable, may also be kinetically limited to moderate temperatures. Keeping in mind these considerations, the best way to demonstrate a transition between equilibrium phases is to demonstrate the reversibility inherent in such a transition.

The purified diblock copolymer fraction of Kraton G-1726 (a commercial polystyrene–poly(ethene-*co*-butene) (S–EB) diblock copolymer containing a small quantity of triblock material) forms a lamellar morphology when cast from tetrahydrofuran (THF) under a range of casting conditions. This lamellar phase remains stable up to 125 °C, which is approximately 55 °C above the glass transition temperature of the short S block. Above this temperature, the material gradually transforms into a cylindrical morphology after passing through an intermediate state. After the cylindrical morphology has formed, subsequent annealing at lower temperatures partially reverses the transformation back to lamellae; full conversion of the cylindrical domains into lamellae is thought to be kinetically limited in this material. We have probed the dynamics of the transition and the structure of the intermediate morphology using in situ small-angle X-ray scattering (SAXS) and transmission electron microscopy (TEM); these results suggest that the process by which one morphology converts into another is a complex, multistep process.

Materials and Methods

Kraton G-1726 commercial block copolymer was obtained from Shell Chemical Co. (Belpre, OH). Literature from Shell reports this material to be a blend of a S–EB diblock copolymer with a S–EB–S triblock copolymer. Size-exclusion chromatography (SEC) with tetrahydrofuran (THF) as the solvent revealed this commercial material to consist of 72% diblock copolymer, 20% triblock copolymer, and high and low molecular weight shoulders.

Repeated fractionation of this material was used to isolate a relatively clean diblock material. A total of 10.5 g of the commercial copolymer was dissolved in a mixture of 3000 mL of toluene and 1000 mL of cyclohexane. Small volumes of methanol were stirred into this solution until the mixture turned turbid.

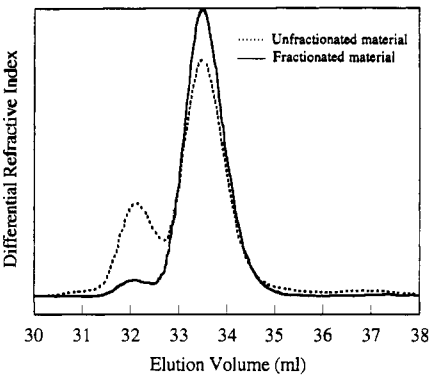

Figure 1. SEC traces for both fractionated and unfractionated Kraton G-1726 diblocks.

The solution was heated to about 70 °C and stirred until the cloudiness disappeared; it was then poured into a large separatory funnel and allowed to cool to room temperature. As the solution cooled, the phase containing the high molecular weight fraction formed at the bottom of the funnel and was removed.

The molecular weight of the fractionated material was determined by SEC in a continuous-porosity, high-resolution, ultrastyragel column set with THF as the solvent. The fractionated material is composed primarily of diblock copolymer with an approximately 5% triblock fraction (of double the diblock molecular weight). By measuring the elution times of a set of narrow-distribution polystyrene standards, as well as a hydrogenated polybutadiene of microstructure similar to that of the EB block in the copolymer, the weight-average molecular weight of the diblock was estimated to be 26 200 with a polydispersity index of 1.05. The SEC profiles for the original and fractionated materials appear in Figure 1.

^{1}H NMR of the fractionated material indicated that the fractionated material is composed of 32 wt % polystyrene and 68 wt % poly(ethene-*co*-butene). The mole fraction of hydrogenated 1,2-butadiene units in the EB block is 0.39 as determined by NMR, corresponding to 12 ethyl branches per 100 carbon backbone atoms. The Flory–Huggins χ parameter has been estimated for a S–EB–S triblock copolymer of similar EB microstructure to be of order 0.1 at 85 °C, falling to 0.08 at 200 °C.[21] The glass transition temperature of the S block was determined by differential scanning calorimetry (Perkin-Elmer DSC-7, heating rate of 20 °C/min) to be 69 °C. Weak melting endotherms from the low levels of crystallinity in the EB block were complete by 45 °C. Estimated χN values for this system range from at least 34 at 69 °C to 28 at the highest temperature examined, 190 °C.

For scattering studies on neat polymer, a sufficient quantity of the fractionated polymer was dissolved in THF to make a 5 wt % solution. A total of 100 μL of this solution was deposited on a clean microscope slide and shaped into a rectangle; surface tension prevented the liquid from spreading. Evaporation of the solvent required approximately 15 min; the resulting film thickness was approximately 300 μm. After removal from the microscope slide, the film was folded repeatedly to form a 1-mm-thick rectangular sample measuring approximately 2 mm by 4 mm. When first placed on the X-ray beam line, films were inserted in a copper sample holder and annealed under vacuum for 10 min at 110 °C to remove any trapped solvent. Diffraction from the sample before and after annealing revealed no change in the microphase of the polymer film.

To confirm preliminary microdomain structure assignment made by X-ray diffraction and to examine the intermediate structures formed during the transition, transmission electron microscopy (TEM) was performed on selected melt-state X-ray samples. After annealing under vacuum on the X-ray line at prescribed temperatures for various times, certain samples were quenched by rapidly returning the sample to atmospheric pressure, removing the sample holder from the thermal stage, and placing the sample holder in liquid nitrogen. Once quenched, the sample morphology is metastable at room temperature. Diffraction from quenched samples revealed no quantitative change in scattering pattern other than an increase in domain

repeat spacings, thus permitting direct structural investigation of the high-temperature microdomain geometry. Quenched samples were microtomed at −125 °C with a Reichert-Jung FC 4E microtome using a diamond knife. To provide image contrast, thin microtomed sections were exposed to RuO_4 vapors (solutions of 0.5 wt % aqueous RuO_4; Electron Microscope Sciences, Fort Washington, PA) for 1–3 min. In contrast to OsO_4, RuO_4 selectively stains the polystyrene domains. The sections of 500–1000-Å thickness were examined using the bright-field mode at 200 kV in a JEOL 200CX electron microscope. Tilt series were obtained using a goniometer stage with ±45° tilt capability. Micrographs were recorded on Kodak SO 163 film and developed in Kodak D-19 at half strength.

X-ray diffraction was used to determine the morphology and lattice dimensions of polymer samples. Cu Kα X-rays were generated from a Rigaku RU-200A rotating-anode X-ray machine equipped with a 0.2 × 2 mm microfocus cathode and Franks mirror optics. Samples were placed inside an evacuated sample chamber and maintained at a temperature of interest by either a pair of thermoelectric devices (temperature range −30 to +175 °C) or a length of nichrome wire inside a copper block (temperature range 20–220 °C). Both thermal devices were controlled to within ±50 mK. Two-dimensional diffraction images were collected with either the Princeton SIT area detector[22] or an image-intensified area detector designed around a Thomson CCD chip.[23] After collection, images were digitized, corrected for detector response characteristics, and then written to magnetic tape. Images were then integrated azimuthally along an arc ±15° from the polymer film normal axis. X-ray diffraction from lamellar phases was characterized by diffraction peaks spaced at ratios of 1:2:3:4:5:... in reciprocal space; typically, 4 or more orders were initially visible in 180-s diffraction exposures from both melt and solution samples after 10 min of annealing at 110 °C. Diffraction from the cylindrical phase was characterized by diffraction peaks spaced at ratios of $1:\sqrt{3}:\sqrt{4}:\sqrt{7}:\sqrt{9}:...$ in reciprocal space; typically, after annealing at high temperatures, four peaks were visible in 180-s diffraction exposures from melt state samples corresponding to the 1st, $\sqrt{3}$, $\sqrt{7}$, and $\sqrt{9}$ orders. The $\sqrt{4}$ peak is suppressed in this material by the cylinder structure factor. Diffraction was taken from a given sample at a fixed interval (usually 0.25, 0.50, or 1.0 h) at a fixed temperature; typical X-ray exposure times ranged from 60 s to 900 s depending on whether higher diffraction orders or time-resolved data were desired.

Kinetic data for the passage of various intermediate phases were estimated from the azimuthally integrated diffraction data. As the difference in lattice spacings between intermediate phases was small, it often proved impossible to resolve the first-order peaks of coexisting lattices. Accordingly, the total intensity of the lowest-order distinguishable peak after the 1st order (2nd order for lamellar systems; $\sqrt{3}$ order for cylindrical systems) was used as a quantitative measure of the total amount of that phase present in the sample.

Results

The S–EB copolymer exhibits an interesting variation in morphology which depends on the solvent from which the film was cast. Samples cast from hexane and cyclohexane, which are strongly preferential for the EB block, show a cylindrical morphology with poorly developed long-range order (as evidenced by weak higher-order reflections and broad peak widths) when examined with X-ray diffraction. The intercylinder spacing, a, for such samples is 242 Å (±5 Å). Annealing such samples at temperatures ranging from 110 to 200 °C for durations of up to 100 h merely improves the long-range ordering of the sample without altering the observed microphase. On the other hand, casting from THF, a nearly nonpreferential solvent for both blocks (see later), results in a lamellar microdomain structure.

The composition of the S–EB diblock places it near the boundary separating the cylindrical and ordered bicontinuous double diamond (OBDD) strong segregation morphologies in the phase diagrams determined for S–I diblocks.[24,25] However, the Flory–Huggins χ parameters are quite different for S–I and S–EB contacts; the statistical segment lengths for poly(ethene-*co*-butene) and polyisoprene also differ. Such differences suggest that S–I and S–EB diblocks of identical minority component volume fractions may not necessarily assume the same equilibrium morphology under identical conditions. Furthermore, as has been previously noted, nonequilibrium microdomain structures can be induced by selective solvents. One would anticipate that, near a morphological boundary, such effects would be enhanced, since only a small variation in the relative volume fractions could change the observed microdomain structure. In order to start an annealing experiment from an equilibrium morphology, it is therefore important to cast the polymer film from a nonpreferential solvent.

A rough estimate of the nonpreferential nature of a solvent for a given block copolymer can be made from the solubility parameter differences between the solvent and the respective blocks. A better, quite sensitive, approach is to find a solvent such that the second virial coefficient, A_2, is the same for each solvent–polymer pair. This, at present, necessitates undertaking a systematic study of various solvents, since to the best of our knowledge no such data exist for EB. A third approach is to select a solvent which gives a similar Mark–Houwink–Sakurada (MHS) exponent[26] for both polymers; this approach has the advantage of relatively many published values. MHS exponents are available for a wide range of solvents with S.[27] No published data are available specifically for EB; however, a number of studies have been made for quite similar model polyolefins created by hydrogenation of anionically synthesized polydienes. One such polyolefin is poly(ethylene-*co*-propylene), or EP. On this basis, THF is a good, relatively nonpreferential solvent for S-EB; the MHS exponents are 0.686 for EP–THF[28] and 0.731 for S–THF.[29]

Samples cast at room temperature from THF exhibit an oriented lamellar morphology in which the lamellae stack preferentially in the plane of the film due to surface effects experienced during casting. The interlamellar spacing for such as-cast films is 295 Å (±5 Å) at 20 °C. Annealing the as-cast sample at temperatures below 130 °C for times of up to 40 h does not produce any morphological transitions. Such treatment merely decreases the interlamellar spacing to 284 Å and increases the long-range lamellar order in the material (as evidenced by a decrease in the widths of the lamellar reflections and the appearance of higher diffraction orders); see parts a and b of Figure 2. Analysis of diffraction amplitudes from the annealed lamellar phase reveals that the styrene block occupies 0.29 ± 0.02 of the unit cell volume at 110 °C. This agrees reasonably well with the value of 0.28 calculated from the material's composition (from ^1H NMR and assuming complete segregation of blocks) and the known densities of S and EB polymers at 110 °C (see Table 1).

A transmission electron micrograph of a sample exhibiting this diffraction signature appears in Figure 2c. The bright-field image shows well-organized lamellae with occasional chevron grain boundaries characteristic of the lamellar morphology.[30]

Annealing of lamellar films at 130 °C or above produces several changes in the microdomain morphology. At annealing temperatures above 130 °C, the orientational order of the lamellar film disappears rapidly. The characteristic time over which this order vanishes is less than the minimum time needed to reach the annealing

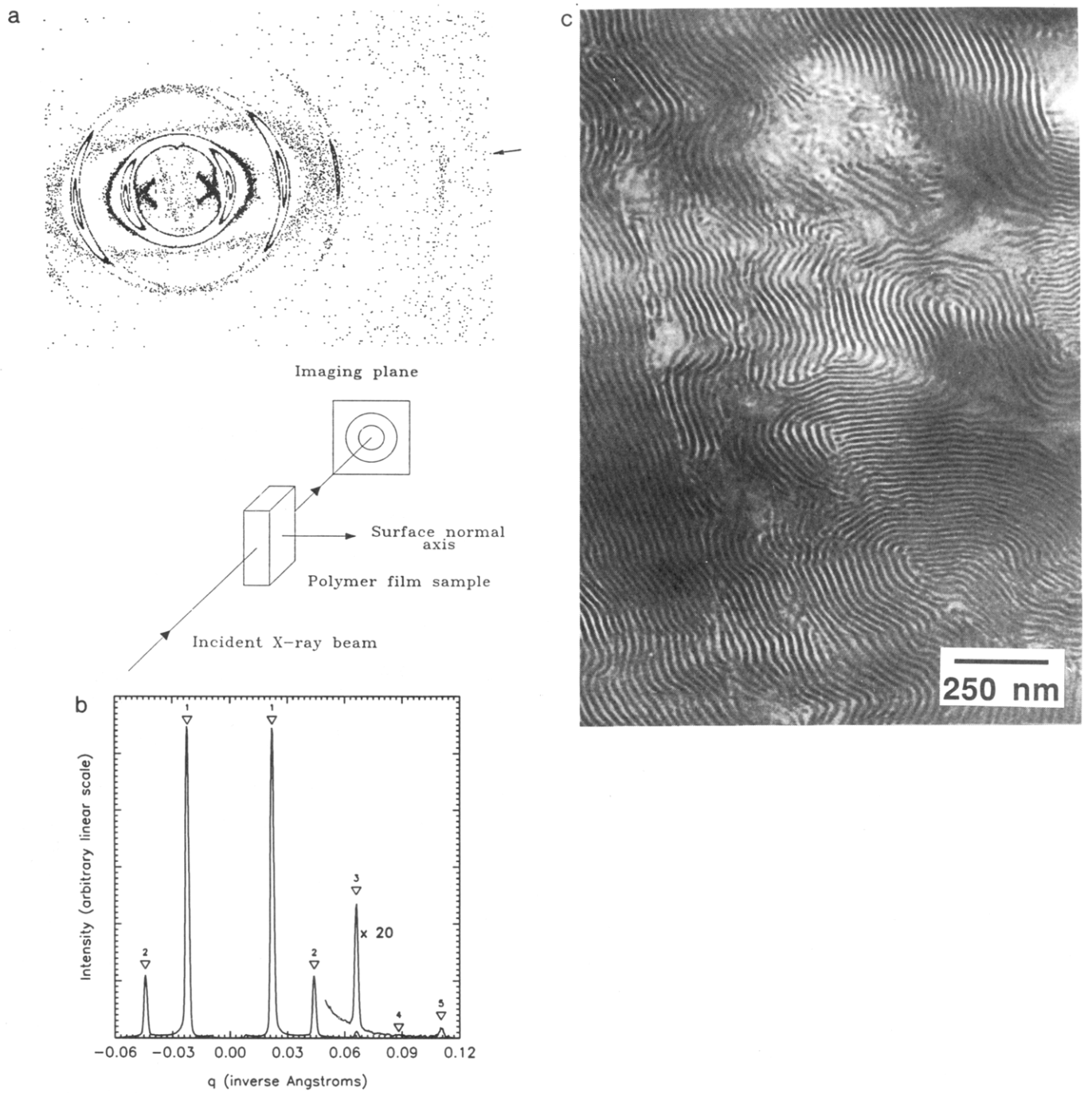

Figure 2. (a) Two-dimensional SAXS image from the diblock film after annealing for 10 min at 110 °C. The exposure time for this image was 10 min. Contours are shown at levels of 15, 100, 1000, and 10 000 arbitrary linear intensity units; one unit corresponds roughly to one Cu Kα X-ray. The concentration of scattered radiation in the direction of the polymer film surface normal axis indicates partial orientation of the lamellae. (b) One-dimensional scattering profile of the two-dimensional image shown in Figure 2a, prepared by integrating the total number of counts at a given distance from the center of the image over a 15° half-angle about the film normal axis. q is defined as $(4\pi/\lambda)\sin\theta$, where 2θ is the angle between the incident and scattered radiation and λ is the wavelength of the incident X-rays. 1–5 denote the expected peak positions for a lamellar morphology; the repeat spacing (d) of this lattice is approximately 284 Å. Analysis of the diffraction amplitudes gives the lamellar unit cell a volume fraction of 0.29 minority component. (c) Transmission electron microscope (TEM) micrograph of a sample annealed 10 min at 110 °C. A well-ordered lamellar morphology (denoted "L" in the text) with some grain boundaries is evident.

temperature from 110 °C and collect a diffraction pattern (120 s). X-ray images taken upon reaching the desired annealing temperature exhibit only powder diffraction rings with little or no azimuthal variation in scattered intensity. Three new diffraction signatures are also observed, indicating reorganization of the molecules in the original lamellar microstructure into a series of new morphologies.

The first new signature appears at temperatures between 130 and 150 °C; it is shown in Figure 3a. After reaching the annealing temperature, the diffracted intensity from the lamellar phase (L) declines rapidly over time; this drop in intensity makes it difficult to accurately measure the lamellar phase spacing after annealing commences. The spacing appears to shrink from its initial value of 284 Å at 110 °C to a value of approximately 250 Å after only a few hours of annealing. Further changes in the lamellar phase spacing are obscured by scattering from a new set of peaks which appear almost immediately upon reaching the annealing temperature. The diffracted intensity from

Table 1. Characteristics of the S and EB Blocks[a]

block	M_w	$\langle R_0^2\rangle/M_w$ (Å^2 g^{-1} mol)	$\langle R_0^2\rangle^{1/2}$ (Å)	ρ (110 °C) (g/cm^3)	ϕ (110 °C)
S	8 400	0.434[36]	60	1.00[36]	0.29
EB-12	17 800	0.989[37]	133	0.80[37]	0.71

[a] M_w = weight-average molecular weight of each block. R_0 = root-mean-square end-to-end distance of an appropriate homopolymer with the same number-average molecular weight. ρ = homopolymer density at 110 °C. ϕ = volume fraction of each block in the copolymer at 110 °C.

these peaks increases rapidly and eventually reaches a maximum; the peak positions do not change with subsequent isothermal annealing. As the annealing temperature increases, the rate of this transformation also increases. The new structure is characterized by three evenly spaced peaks in reciprocal space; the third peak is extremely weak and is observed only sporadically. Such diffraction is consistent with a lamellar morphology, but X-ray diffraction alone does not provide sufficient information to definitively identify the structure. At temperatures above 140 °C, identification of cleanly separated peaks belonging to the two lattices becomes difficult, and at temperatures above 150 °C, transformation of the lamellar phase into the new structure occurs so rapidly that the diffraction signature just described is not observed.

Transmission electron micrographs of a sample exhibiting this diffraction signature appear in Figure 3b. Two types of image contrast variations are visible. The first type of region (L) exhibits the characteristic lamellar signature of alternating bands of light (EB) and dark (S) domains, with sharp interfaces separating the light and dark regions. This region therefore corresponds to the original lamellar morphology. The second type of region (ML) displays a variable contrast within the dark layers which alternate with uniform light layers. Several possibilities could account for the observed contrast variation of the dark RuO_4-stained S regions. A lamellar-catenoid structure occurring with the catenoid axes across the S domains is one possibility;[31-33] alternatively, the S lamellae may undergo a transformation to cylinders with their long axes lying in the plane of the original lamellar S domain. A schematic of the second proposed structure appears in Figure 4a. Depending on the relative orientation of the ML grain, one observes discrete S cylinders when viewed end-on, modulated S layer contrast for oblique views, and uniform S layer contrast for transverse (90°) projections (see parts b and c of Figure 4). As it is impossible to obtain uniform S layer contrast in a projection of the lamellar-catenoid structure, the second interpretation proposed above is consistent with the appearance of the S regions in the TEM tilt series, while the first interpretation is not.

It is important to note that ML grains do not contain a well-developed hexagonally ordered packing of S cylinders in an EB matrix; this would be clearly evident in [001] axial projections of the structure. The image constrast variations also suggest a periodic intrasheet spacing of the S cylinders but with cylinders in adjacent sheets out of register with one another. This disorder accounts for the absence of the $\sqrt{3}$ and $\sqrt{7}$ reflections in the SAXS pattern; it also suggests that the lamellar-like Bragg diffraction from the new structure arises primarily from the regular packing of the sheets and not from the cylinders that compose the sheets. We therefore denote the diffraction signature which corresponds to this microstructure lamellar/modified layer (L/ML). Individual cylinders appear to form in the plane of a given lamella; distortions in the S–EB interface of a lamella in the vicinity

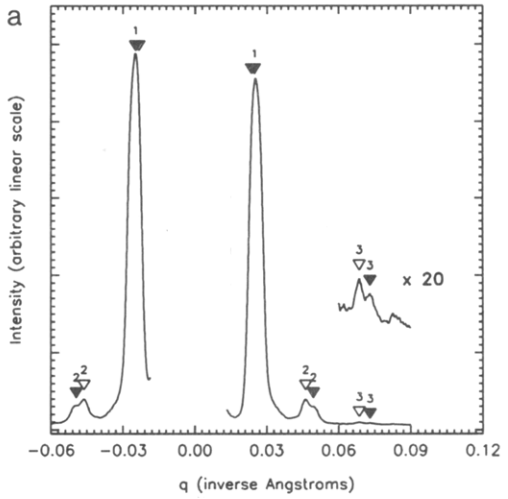

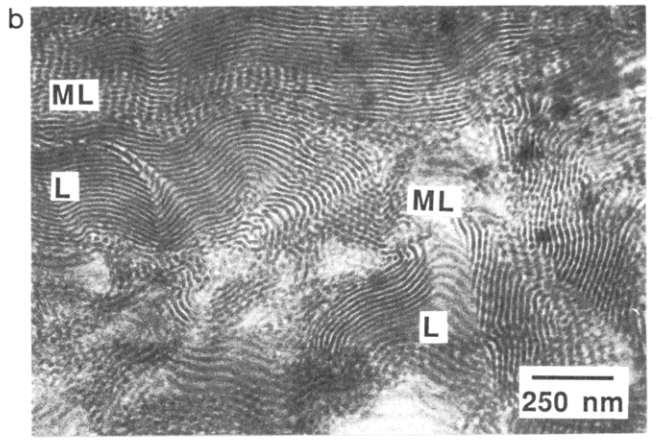

Figure 3. (a) One-dimensional scattering profile of the first diffraction signature, denoted "L/ML" on the basis of electron microscopy results. This particular image was obtained after 4 h of annealing at 135 °C. Expected peak positions for the original L lattice are indicated with hollow triangles; expected positions for the new ML lattice are indicated with filled triangles. The basis vector lengths for these two lattices are 272 (L) and 255 Å (ML) in this sample. The two-dimensional image from which this profile was constructed shows no significant variation in scattered intensity as a function of azimuthal angle, indicating that the orientation in the original lamellar lattice has disappeared. (b) TEM micrograph of a sample annealed for 50 h at 130 °C. Both the original lamellar (L) morphology and a new structure, the modified layer (ML) structure, are observed. The second geometry consists of sheets of parallel cylinders with a well-defined nearest-neighbor spacing between the cylinders in each sheet. Cylinders in adjacent sheets are out of register with one another, giving rise to layerlike ordering and causing the structure to diffract essentially as a lamellar morphology.

of a cylindrical domain suggest that some sort of interfacial instability may drive the transformation.

Heating the film from 110 °C to temperatures between 150 and 175 °C produces the second diffraction signature (shown in Figure 5a); this signature also appears in samples annealed at lower temperatures after the disappearance of the L/ML signature. Both the modified layer and a new structure form immediately upon reaching the annealing temperature. Weak, poorly defined scattering peaks appear at spacing ratios of $1{:}\sqrt{3}{:}\sqrt{7}$, suggesting that the new structure is a cylindrical morphology in which the cylinders pack on a hexagonal lattice. A reflection at a spacing corresponding to $\sqrt{9}$ is occasionally observed as well. The equilibrium d-spacing of the new lattice decreases with increasing annealing temperature (see Table 2). The characteristics of the X-ray optical system prevent resolution of the different first-order peaks of the

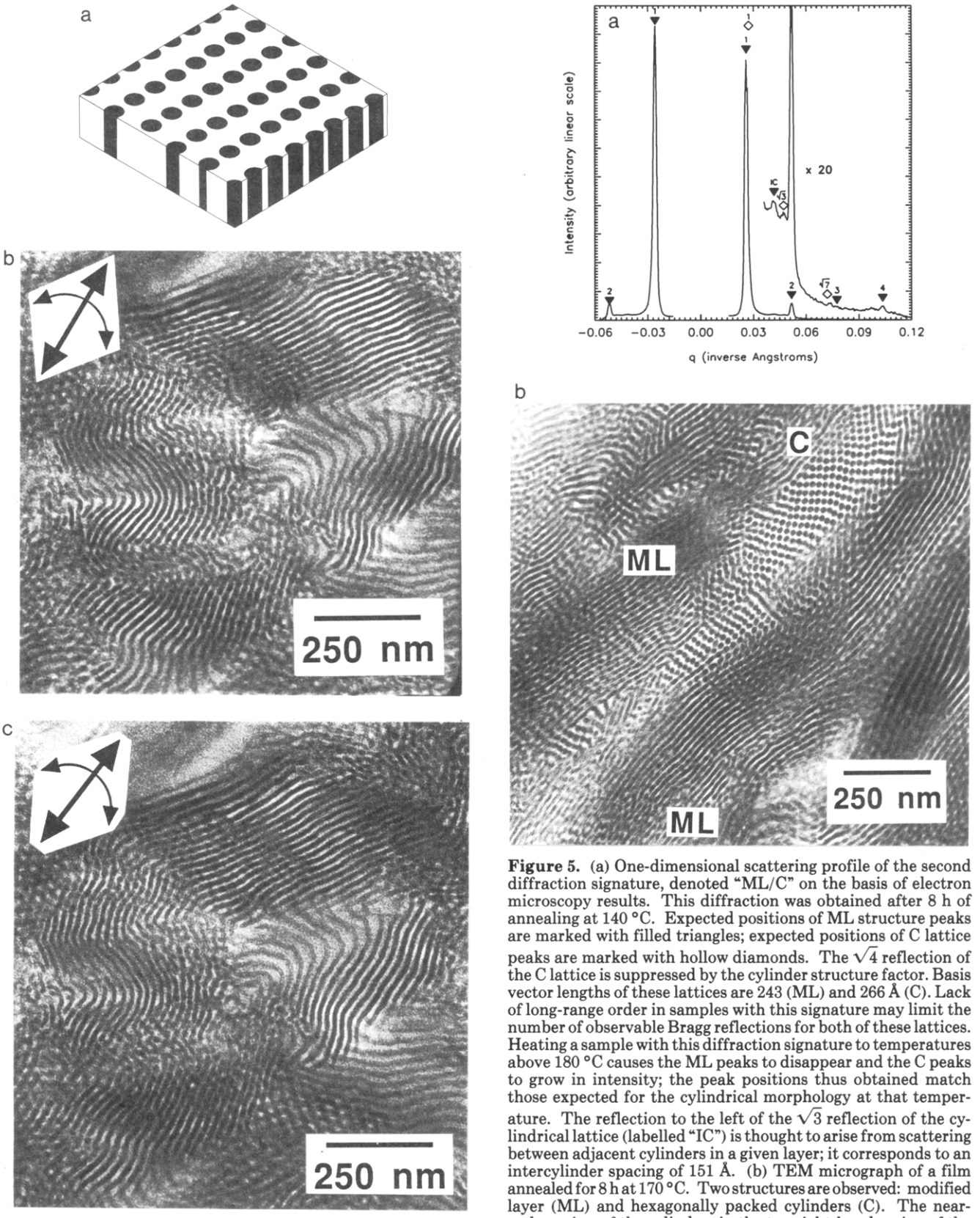

Figure 4. (a) Modified layer (ML) structure. Cylinders of the minority component are shown in black; the surrounding matrix of the majority component appears in white. The position of cylinders in adjacent layers are uncorrelated, implying a lack of long-range order along the direction normal to the layers. (b and c) Tilt pair of TEM micrographs of a region containing both L and ML structures. The tilt between the two images is 10° clockwise about the axis shown in the inset for Figure 4b. Changes in image contrast in the ML regions are consistent with an oblique projection through layers of cylinders.

Figure 5. (a) One-dimensional scattering profile of the second diffraction signature, denoted "ML/C" on the basis of electron microscopy results. This diffraction was obtained after 8 h of annealing at 140 °C. Expected positions of ML structure peaks are marked with filled triangles; expected positions of C lattice peaks are marked with hollow diamonds. The $\sqrt{4}$ reflection of the C lattice is suppressed by the cylinder structure factor. Basis vector lengths of these lattices are 243 (ML) and 266 Å (C). Lack of long-range order in samples with this signature may limit the number of observable Bragg reflections for both of these lattices. Heating a sample with this diffraction signature to temperatures above 180 °C causes the ML peaks to disappear and the C peaks to grow in intensity; the peak positions thus obtained match those expected for the cylindrical morphology at that temperature. The reflection to the left of the $\sqrt{3}$ reflection of the cylindrical lattice (labelled "IC") is thought to arise from scattering between adjacent cylinders in a given layer; it corresponds to an intercylinder spacing of 151 Å. (b) TEM micrograph of a film annealed for 8 h at 170 °C. Two structures are observed: modified layer (ML) and hexagonally packed cylinders (C). The near-end-on view of the cylinders in the top right-hand region of the micrograph shows well-developed packing of the cylinders into a two-dimensional lattice with hexagonal symmetry. The ML regions show no lateral symmetry of cylinders across adjacent layers.

ML and new lattice. The observed "first-order" peak, though, is well-represented as a superposition of two Gaussian peaks located at the positions determined by the higher-order peaks of the ML and new lattices.

Table 2. Variation in Unit Cell Dimension with Annealing Temperature

temp (°C)	*d*-spacing[a] (Å)			
	lamellar	mod layer	intercylinder[b]	cylindrical[c]
110	284			
130		250		
135		247		
140		243	151	268
145		240	151	270
150		242	150	260
160		238		254
170		235		251
180				250
190				246

[a] Lamellar phase spacing at 110 °C is uncertain to ±2 Å. All other spacings are uncertain to ±5 Å due to variation across samples. [b] Distance between adjacent cylinders within a given layer. At higher temperatures, the cylindrical phase developed so rapidly that sufficient long-range order to produce this diffraction peak did not develop. [c] Distance between adjacent cylinders in the hexagonal lattice, usually denoted *a*.

Due to the weakness of the diffraction, X-ray measurements alone are not sufficient to determine the morphologies present in samples which produce the second signature. The microstructure assignments proposed above are supported by electron microscopy, however. The bright-field TEM image of Figure 5b shows regions of relatively disordered cylinders (characteristic of the ML structure) coexisting with regions of hexagonally packed cylinders (characteristic of the cylindrical morphology, abbreviated C). The second diffraction signature is therefore denoted modified layer/cylinders, or ML/C.

After considerable annealing time at low temperatures within this temperature range, a new peak often appears between the first X-ray reflection of the modified layer lattice and the $\sqrt{3}$ reflection of the cylindrical lattice in the ML/C signature (Figure 5a). This peak has been marked "IC". We interpret this peak as arising from coherent scattering between neighboring cylinders within each layer. The radii of the styrene cylinders within the coexistence ML and C phases can then be estimated from the volume fraction of the styrene component of the copolymer and the dimensions of both unit cells; the values typically agree to within 10%. At low annealing temperatures within this temperature range, the diffracted intensities of the ML and C structures remain constant over time. At higher annealing temperatures, the diffracted intensity of the ML structure declines slowly over time while the intensity of the C phase grows. In this case, the new peak does not appear. As in the case of the L/ML signature, the total time over which the ML and C signatures coexist decreases as the annealing temperature rises, and at temperatures above 160 °C, detection of the ML structure becomes difficult.

Between 150 and 175 °C, the two intermediate diffraction signature already discussed appear only rarely; above 175 °C, they are never observed. Instead, upon heating the film to the annealing temperature, a set of peaks corresponding to a cylindrical morphology are recorded; the peak positions match those of the C phase in the intermediate signature ML/C. Typically, four or more diffraction orders are observed, with positions in the ratio of $1:\sqrt{3}:\sqrt{7}\sqrt{9}$; a typical diffraction pattern is shown in Figure 6a. An electron micrograph of a sample with this diffraction signature quenched from 190 °C appears in Figure 6b. The bright-field image contrast shows both well-ordered axial and transverse projections of hexagonally packed S cylinders.

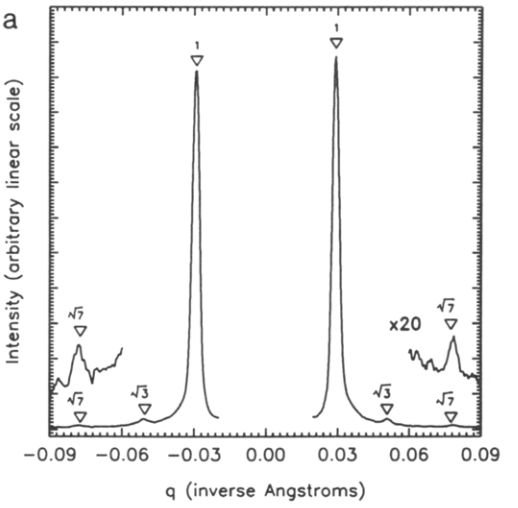

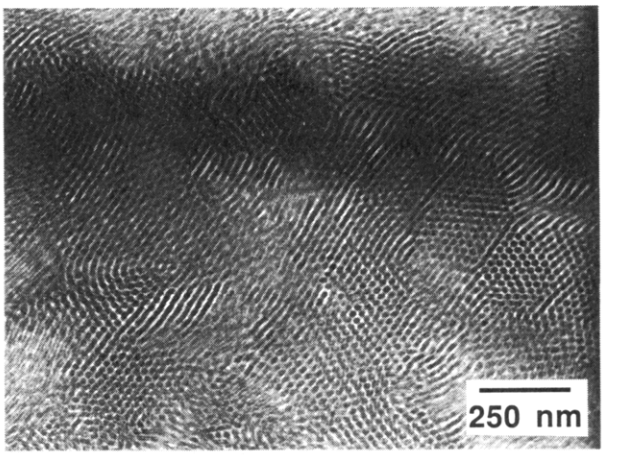

Figure 6. (a) One-dimensional scattering profile for the cylindrical phase; this particular profile was taken after 1 h at 190 °C. As noted previously, the $\sqrt{4}$ reflection from this lattice is suppressed by the cylinder structure factor. The peak positions shown here nearly match those recorded for the C morphology in the intermediate signature ML/C; the slight discrepancy observed is attributed to the decrease in the lattice spacing with increasing temperature. The intercylinder distance, *a*, for this lattice is 245 Å. (b) TEM micrograph of a film annealed for 15 min at 190 °C. In addition to axial views, all oblique views of the hexagonal lattice of well-ordered cylinders (the C morphology) show good registry of the cylinders.

Although the qualitative characteristics of the diffraction signatures, including the temperatures at which they were observed and the sequences followed by the signatures over time at a given temperature, were repeated across several samples at each temperature, characteristic times for the growth or decay of the lattices composing the signatures proved difficult to obtain. Characteristic times for changes in *d*-spacings also proved difficult to obtain. Measured values of peak intensities for the lattices did not display consistent numerical trends across several samples at the same temperature; attempts to estimate characteristic times for the growth or decay of these structures produced widely varying and often contradictory results. Finally, the weak intensity of the higher-order peaks makes it difficult to say when a given microstructure completely disappears from the diffraction signature. These difficulties preclude any precise statements regarding the dynamics of these transformations. Nonetheless, certain qualitative observations are possible. Figure 7 summarizes the observed diffraction signatures

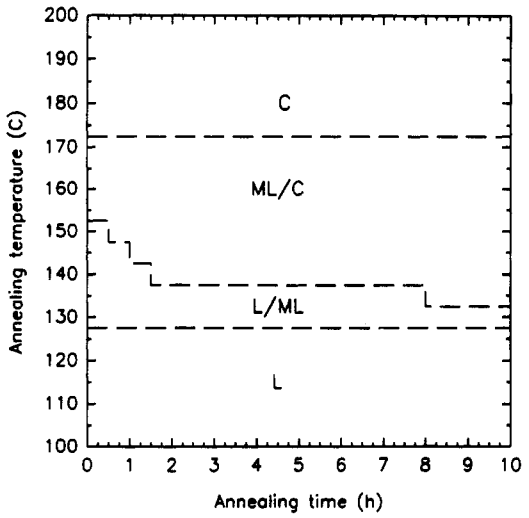

Figure 7. Observed diffraction signature in S–EB diblock films as a function of annealing temperature and annealing time. L denotes the original lamellar lattice. The L/ML signature results from the coexistence between the original lamellar lattice and a structure composed of parallel sheets of cylinders. The ML/C signature results from coexisting domains of cylinders arranged in parallel sheets and domains in which cylinders pack on a hexagonal lattice. C denotes an array of hexagonally packed cylinders. As described in the text, the considerable variation in sample behavior at high temperatures makes it difficult to locate a boundary separating the ML/C regime from the C regime; the boundary was arbitrarily located at the position above which the ML/C signature has not been observed. The lines separating the phases in the horizontal direction (time) are intended as guides to the eye only; at each temperature, samples exhibited considerable variation in dynamic behavior as described in the text.

as a function of increasing temperature and time over the range of values studied.

The dimensions of the unit cells of each morphology as determined by X-ray diffraction appear in Table 3. The dimensions of the S and EB domains within each lattice were estimated from the data shown in Tables 1 and 2 and the volume fraction of the styrene block (as estimated from the diffraction peak amplitudes). From these values, the interfacial area per S–EB junction and the mean lengths of the S and EB chains were calculated for the four observed morphologies (L as cast, L after annealing, modified layer ML, and C); these results also appear in Table 3.

Table 3. Structural Dimensions of the Observed Microphases

phase	Bragg spacing (Å)	vol of S block (Å^3)[a]	thickness (Å)[b] S domain	thickness (Å)[b] EB domain	interfacial area (Å^2)[c]
L	295[d]	13 000	43	104	300
	284[e]	13 700	41	101	334
ML	242[f]	14 000	58	107	483
C	250[g]	14 400	61	112	472

[a] Calculated from the measured M_w of the S block and the density of S at the temperature of interest.[38] [b] For the lamellar morphology, the length quoted is the half-thickness of the appropriate domain. For the nonlamellar morphologies, the length quoted for the S chain is the radius of the cylinder core; the length of the EB block is the distance between the cylinder core and an ideal cylindrical corona layer with the same minority component volume fraction as the block copolymer. [c] Calculated from the volume of the S block and the dimensions of the S domain. [d] Immediately after casting; SAXS data taken at 20 °C. [e] After 10 min of annealing at 110 °C; SAXS data taken at 110 °C. [f] Typical value at 150 °C. [g] Intercylinder spacing, usually denoted a.

Discussion

Recently, Sakurai *et al.*[18] have presented a study of a nonequilibrium cylinder-to-lamellae order–order transition in a styrene–butadiene–styrene triblock copolymer (56 wt % styrene), as examined by SAXS and TEM. By casting from methyl ethyl ketone, which is a selectively good solvent for polystyrene, a morphology of butadiene cylinders in a styrene matrix was produced which spontaneously relaxed to lamellae upon heating to 158 °C. However, the evolution of their SAXS data differs from what we have observed; in their experiment, peaks from initial cylindrical lattice gradually vanished, and subsequently reflections characteristic of the lamellar phase emerged and grew in intensity. At no time could peaks from two coexisting phases be discerned, presumably because the grains of these coexisting phases, if they existed, were only a few Bragg spacings in size. In our case, peaks from coexisting L/ML and ML/C structures could be clearly observed for suitable time–temperature combinations (see Figures 3a and 5a); coexisting L/ML and ML/C structures also appeared in TEM images of samples exhibiting these diffraction signatures (see Figures 3b and 5b).

In another recent study, Hamley *et al.*[34] have identified two new structures, hexagonally modified lamellae and hexagonally perforated lamellae, in a morphological transition from the lamellar to the cylindrical phase in a weakly segregated poly(ethylenepropylene)–poly(ethyethylene) (EP–EE) diblock copolymer. Their measurement suggests that the new structures are equilibrium morphologies. In contrast to our work, which employed a relatively short polymer composed of blocks with a high χ value, their experiments used block of much higher molecular weight and lower χ value; the minority component volume fractions (f) of the two diblocks also differ. Comparison between the two sets of results are therefore difficult to make: it is not surprising that the two new morphologies were not observed in the S–EB system examined here.

Comparison of the respective domain sizes for S and EB in the lamellar phase and the modified layer structure indicates the order–order transition is initially driven by chain deformation energy. In the pure diblock the S domain length increases from 41 to 58 Å on going from the lamellar to the modified layer structure; this value is very nearly equal to the unperturbed root-mean-square end-to-end distance of the 8400 molecular weight S block at 110 °C, 60 Å.[35,36] At the same time, the EB domain length increases slightly from 101 to 107 Å. As the unperturbed root-mean-square end-to-end distance of the 17 800 molecular weight EB block at 110 °C is approximately 133 Å,[37] assumption of the ML structure by the block copolymer forces the EB block to adopt a "compressed" configuration and spread along the S–EB interface. The variation in the chain dimensions as the transition progresses forces a large change in the interfacial area per junction point and in the interfacial curvature (see Table 3).

As can be seen in Figure 3b, the L-to-ML transformation propagates more rapidly parallel to the lamellar surface than it does along the lamellar normal, indicating that neighboring lamellae are not strongly coupled. Some coupling must exist, however, since the axes of cylinders which form in adjacent lamellae are usually parallel. For the lamellar structure to transform directly to the equilibrium hexagonal packing of cylinders, the wavevectors of the shape fluctuations in adjacent lamellae must be parallel and 180° out of phase. If adjacent lamellae are not so tightly coupled, then the original lamellar structure might be expected to transform initially into one in which

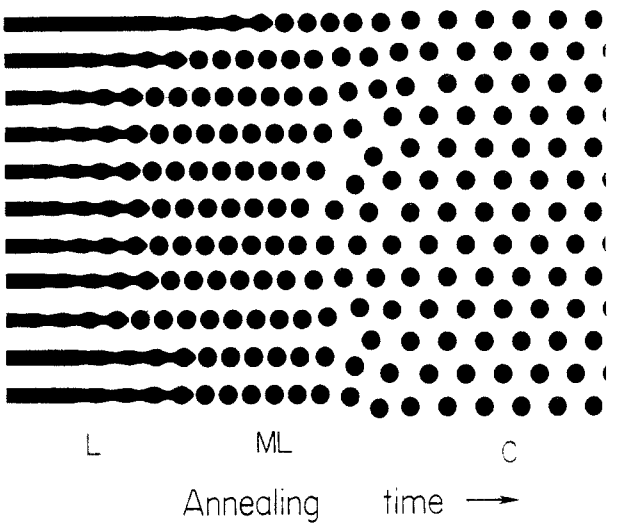

Figure 8. Schematic of the transition from lamellae to cylinders. S domains appears in black; EB domains appear in white. The transition is a two-step process: lamellae (L) transform into layers of disordered cylinders (ML), which subsequently reorganize into the hexagonal packing characteristic of the cylindrical phase (C).

the cylinders formed in adjacent lamellae were in poor register. Such a morphology, which we identify with the modified layer structure, would diffract essentially as a lamellar phase in specimens without preferred orientation. Subsequently, this geometry would reorganize to one in which the cylinders were hexagonally arranged. Figure 8 depicts the morphologies encountered as lamellae transform into cylinders by means of the two-step sequence outlined above.

X-ray scattering data indicate that reorganization of the styrene cylinders in the modified layer structure into the hexagonal packing characteristic of the cylindrical morphology involves relatively little change in the interfacial area per junction or radius of the styrene cylinders. In order for the segmental density of EB to remain constant throughout the region surrounding the styrene cylinders, the EB chains must stretch perpendicular to the S–EB interface to fill the interstitial regions at the corners of both the modified layer and cylindrical unit cells. The chains must also spread parallel to the same interface to maintain a constant density in the narrow region separating adjoining cylinders (see Figure 9). Such configurational anisotropy necessarily involves a loss of entropy for the EB chains; this loss is greater in the modified layer structure, where the degree of stretching and spreading is larger, than in the cylindrical phase. It is reasonable to assume that this difference in entropy drives the reorganization of the modified layer structure into the cylindrical phase. The rate at which this reorganization occurs depends on many factors, including the amount of disorder present in the initial layer microstructure, the nature of the stresses at grain boundaries, and the temperature of the sample. The first two factors may vary considerably from grain to grain within the sample, leading to a broad distribution of relaxation rates and hence a broad distribution of grain lattice dimensions at any given time. Such a distribution gives rise to X-ray diffraction characterized by broad first-order peaks and weak or absent higher-order reflections. This accounts for the difficulties observed in identifying the modified layer structure at low annealing temperatures. This may also account for the difficulty in obtaining reproducible kinetic data for the morphological transformations, as the grain size distribution is not well-controlled across different samples. As the annealing temperature increases, variations in the local

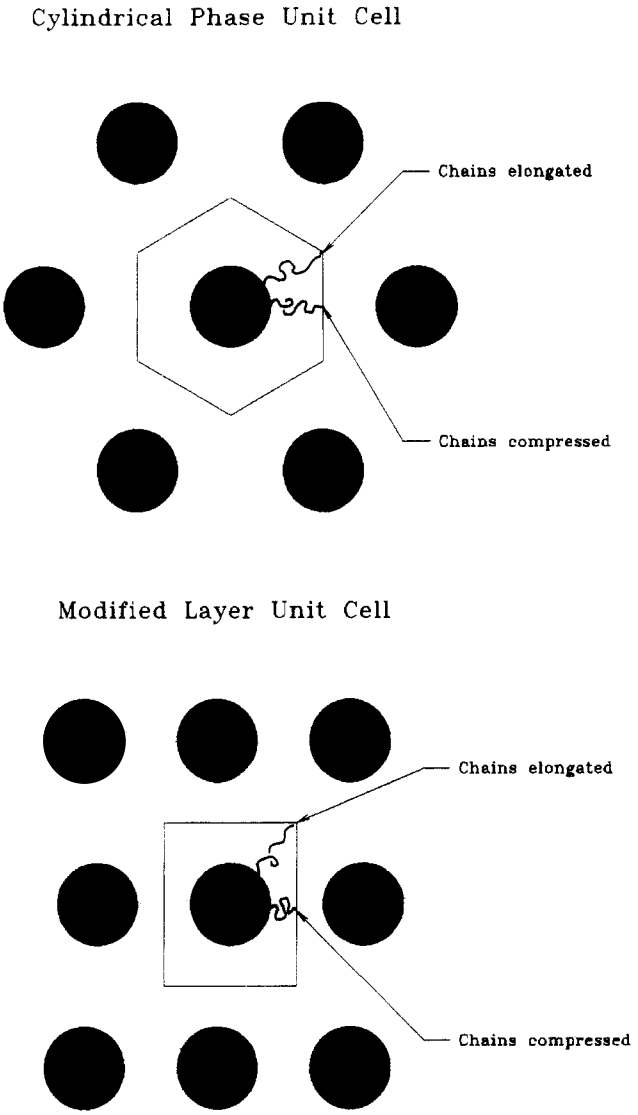

Figure 9. Illustration of the entropic cost of chain packing anisotropy. As in the electron micrographs, the S cores of both morphologies are shown in black while the EB matrix surrounding the cores is shown in white. Chains with interfacial junction points located opposite the corners of both unit cells are elongated (relative to chains with junction points on either side) in order to maintain a constant segmental density throughout the matrix region. Similarly, chains with junction points located on or near the lines joining adjacent cylinders are compressed in order to maintain a constant segmental density. This anisotropy for the configurations adopted by the EB chains in different locations within both unit cells implies a loss of configurational entropy; the loss is greater in the modified layer geometry, where the degree of elongation and compression is greater.

environment of each grain become less significant and the importance of the difference in configurational entropies discussed earlier increases. Consequently, the distribution of lattice structures narrows, the quality of the X-ray diffraction (as measured by peak widths and the presence of higher-order diffraction orders) improves, and the rate of reorganization into the hexagonal packing increases.

It is important to ask whether the transition in our material from lamellae to cylinders represents a thermotropic order–order transition similar to those observed in other microphase-separated systems (such as phospholipid–water dispersions) or is instead the relaxation of a nonequilibrium morphology caused by a selective solvent. As noted previously, for samples whose composition locates them on a phase boundary separating different morphologies, the presence of even a slightly selective solvent may be enough to induce the formation of a nonequilibrium

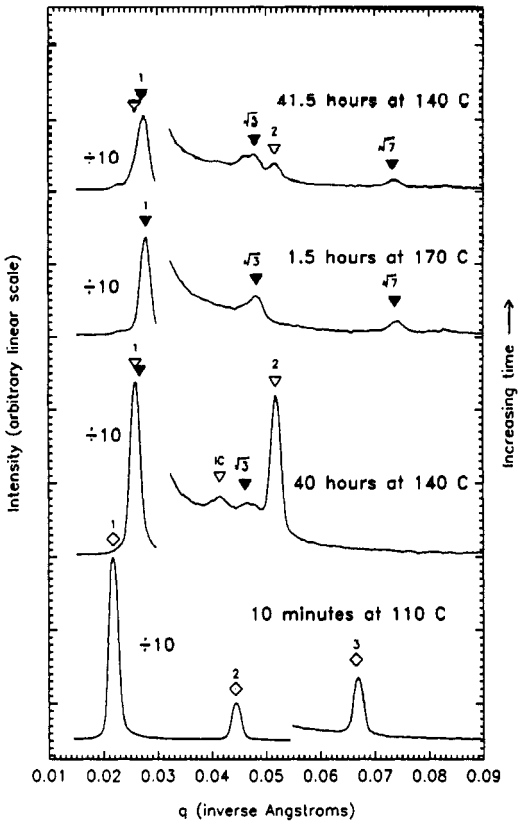

Figure 10. One-dimensional SAXS profiles of a melt-state S–EB film treated with an unusual annealing protocol. Peak positions for the original L morphology are indicated with hollow diamonds; positions for the ML morphology are indicated with hollow triangles; and positions for the C morphology are indicated with filled triangles. After casting, the film was annealed for 10 min at 110 °C to remove residual solvent; diffraction indicates a lamellar phase was present. As seen from the figure, 40 h of heating at 140 °C produced coexisting ML and C morphologies; 1.5 h of subsequent annealing at 170 °C caused the conversion of all ML domains to C domains; and returning the sample to 140 °C caused the appearance of a new morphology after 41.5 h. Subsequent annealing for 40 h at 120 °C caused no further changes in the scattering profile apart from a slight change in the repeat spacing of both lattices. Although the diffraction from the new morphology is consistent with the ML structure (as indicated by the hollow triangles), it is also consistent with a lamellar morphology; the new structure cannot therefore be identified by X-ray scattering alone.

microstructure. Perfectly nonselective solvents do not exist in practice; assessment of these solvent effects must be performed before statements about "equilibrium microstructure" can be made.

Perhaps the only way to ensure the elimination of solvent effects is to employ a block copolymer with a sufficiently small value of χN so that the sample may be raised into the homogeneous disordered state and then quenched and held isothermally to follow the evolution of microdomain ordering at a particular temperature. Kinetic effects may slow or stop ordering at low temperatures, however. A better way to determine the nature of the transition is to examine reversibility. Thermally induced transitions between equilibrium microstructures should be thermally reversible (though kinetic effects may impede transitions at low temperatures), while transitions from a nonequilibrium morphology to the equilibrium one should not be reversible.

Figure 10 depicts a series of one-dimensional SAXS profiles for a melt-state sample with an unusual annealing history. After casting, the film was annealed for 10 min at 110 °C; SAXS diffraction produced peak spacings indicative of a lamellar morphology. Next, the film was annealed for 40 h at 140 °C; diffraction signatures for the ML and C morphologies were observed. After 1.5 h of further annealing at 170 °C, diffraction indicated complete transformation of the microstructure to the cylindrical morphology. In an attempt to reverse this transition, the temperature was then lowered to 140 °C and the sample was annealed for an additional 41.5 h. In addition to the diffraction signature of the C phase, scattering peaks were observed at positions in reciprocal space which corresponded to the positions observed previously for the ML state at 140 °C; the lower intensity of the new second-order reflection when compared to the initial exposure at 140 °C presumably indicates that less of the noncylindrical state is present at this time. Since both the ML state and L morphology give identical peak position ratios of 1:2:3:4:..., the new structure cannot be determined on the basis of X-ray diffraction alone. The peak positions for the C lattice signature precisely match those measured in the heating scan taken previously. Subsequent annealing of similarly treated samples for 40 h at 120 °C did not produce further changes in morphology as determined by SAXS; kinetic effects at this low temperature may have impeded further transformation of the cylinders. Such effects may also have accounted for our failure to observe a transformation from the (nonequilibrium) cylindrical phase induced in films cast from cyclohexane to the (equilibrium) lamellar phase after annealing.

The reappearance of a noncylindrical phase at 140 °C in samples which (previously) displayed only cylindrical phase diffraction at 170 °C indicates that the new structure has formed at the expense of the high-temperature cylindrical phase and, hence, that the C phase is not in thermal equilibrium in these samples at 140 °C or below. Even if a small fraction of the sample volume at 170 °C was occupied by domains of a noncylindrical morphology, these domains grew from an undetectable amount at 170 °C to occupy a significant fraction of the sample volume at 140 °C, indicating that they are energetically favored at the lower temperature over the C phase.

Transmission electron micrographs of a partially reversed sample (taken after completion of the annealing sequence described above, including annealing at 120 °C) appear in parts a and b of Figure 11. Depending on the region of the film chosen for examination, one observes large domains of either hexagonally packed cylinders or lamellae. The new morphology observed with X-ray scattering at 120 °C is therefore a lamellar phase. The reappearance of the lamellar morphology upon cooling to the temperatures at which the lamellar phase was observed upon heating demonstrates that the transition is thermally reversible between two equilibrium morphologies, a result that is impossible to achieve in a nonequilibrium transition.

While detailed examination of the C-to-L transition lies outside the scope of this paper, we note that this transition appears to proceed without the formation of any long-lived intermediate structures. In particular, the intermediate "zipper" structures proposed by Sakurai *et al.*[18] (formed by neighboring cylinders which zipper together along the [10], [11], and [1$\bar{1}$] directions to form short, bent lamellae) were not observed in micrographs of coexisting lamellar and cylindrical phases. This result does not necessarily provide grounds to reject the "zippering" mechanism: if both zippering and subsequent initial annealing of short, bent lamellae into less wrinkled structures occur rapidly, the probability of observing a pair of cylinders transforming into a lamella is extremely low.

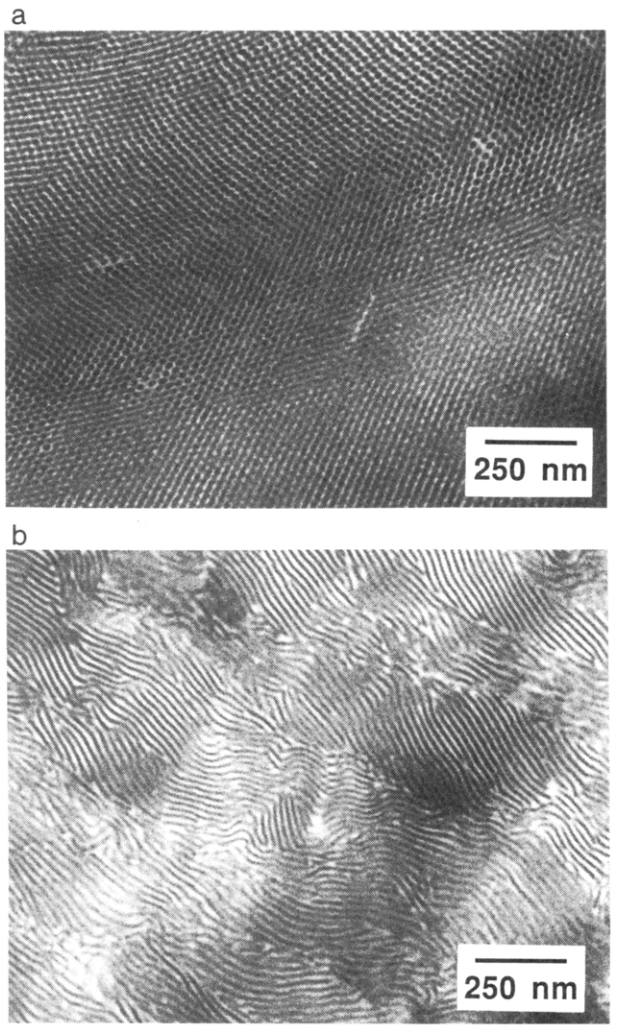

Figure 11. TEM micrographs of a partially reversed sample treated with the annealing protocol described in the caption to Figure 10. Large regions of well-ordered cylinders (a) and well-orderd lamellae (b) are evident. The reappearance of the original lamellar morphology indicates that the lamellar-to-cylindrical transition is reversible.

In view of the number of new block copolymer microstructures proposed in recent years, it is only natural to ask whether the ML state is an intermediate structure which forms during the L-to-C transition or is instead a new equilibrium morphology. The considerable variation in dynamic behavior and transition temperatures across samples (discussed earlier) makes it difficult to answer this question. At isothermal annealing temperatures above 130 °C, samples originally composed of coexisting L and ML regions gradually transform to coexisting ML and C domains (see Figure 7). Such behavior is difficult to explain if the ML structure is interpreted as an equilibrium morphology in this temperature range; it is consistent with a view of ML as a long-lived intermediate state. It is possible that the ML state is in equilibrium in a narrow range about 130 °C, as coexisting L and ML regions persist upon isothermal annealing at this temperature for at least 50 h without converting to coexisting domains of ML and C structures, but it is more likely that such persistence is due to the extremely slow kinetics observed in this temperature range. Finally, it is not clear what thermodynamic forces would drive the cylindrical morphology to transform into an equilibrium ML "phase" as the temperature is lowered. Given these observations, the ML structure is best interpreted as an intermediate structure which forms during the L-to-C transition is this material.

This interpretation leaves one aspect of the system's behavior unexplained, however. As discussed earlier, the appearance of a noncylindrical diffraction signature at 140 °C in (previously homogeneous) C phase samples demonstrates that the cylindrical morphology is not in equilibrium at (or below) 140 °C. The disappearance of the original lamellar morphology upon heating suggests that the lamellar morphology is not in equilibrium above 130 °C, after variation in sample behavior is taken into account. Taken together, these observations suggest that the ML structure (or a new unidentified morphology) is in equilibrium between 130 and 140 °C; unfortunately, this is inconsistent with the observed annealing behavior of samples in the upper half of this temperature range. At the present time, we are unable to account for this contradiction; with further work on the dynamics of the C-to-L transition, it should be possible to determine the nature of the ML state and construct a true phase diagram for this material.

Although all data presented here were obtained with the diblock fraction of Kraton G-1726, initial measurements with the commercial material (which contains a substantial triblock component) produced quite similar results. Sakurai *et al.*[19] have also observed the transformation of a lamellar phase into a cylindrical phase in Kraton G-1652, a polystyrene–poly(ethene-*co*-butene)–polystyrene triblock copolymer which is very nearly the ABBA triblock analog of the AB diblock used in our study. The temperature ranges of all of these measurements were comparable, suggesting that the order–order transition process is not substantially more difficult when the material has a triblock as opposed to a diblock architecture.

Conclusion

The existence of a reversible, thermally driven microphase transition between the lamellar and cylindrical morphologies was demonstrated with self-consistent SAXS and TEM measurements. The transformation from lamellae to cylinders appears to proceed in two distinct steps. Initially, fluctuations at the interface separating the minority and majority component blocks drive the PS lamellae to break up into a partially disordered array of PS cylinders (the modified layer structure) in which the spacing separating adjacent cylinders within each layer remains well-defined. Subsequently, the layers of cylinders anneal into a hexagonally packed geometry. The presence of other proposed intermediates between the lamellar and cylindrical phases (such as the catenoid-lamellar structure, hexagonally modulated lamellae, and hexagonally perforated lamellae) was ruled out by a TEM tilt series performed on selected X-ray samples; this tilt series also confirmed the phase assignments made by X-ray diffraction. The OBDD morphology, which earlier work has located between the lamellar and cylindrical morphologies in the strong segregation regime on the equilibrium morphology diagram for S–I block copolymers, was also not observed. The reverse transformation (from cylinders to lamellae) appears to proceed without passing through any intermediate structures, although additional work is needed in this area to determine the phase diagram of the system and establish the nature of the intermediate phase appearing during the L-to-C transition. However, the complete conversion of all domains in the sample to the cylindrical phase upon annealing at high temperatures, and the reappearance of the original lamellar morphology when the sample is subsequently cooled to lower annealing temperatures, demonstrates that the transition is thermally reversible and hence that the two morphologies are in equilibrium at different temperatures.

Acknowledgment. D.A.H. acknowledges the support of a National Science Foundation Graduate Fellowship. R.J.A. acknowledges the support of the Wolfson Fellowship, given by the Israel Academy of Sciences and Humanities. R.A.R. acknowledges the support of the donors of the Petroleum Research Fund, administered by the American Chemical Society (23792-G7), and the National Science Foundation, Polymers Program (Grant DMR-9257565). Work in the Physics Department of Princeton University was supported by a grant from the U.S. Department of Energy (DE-FG02-87ER60522-A000). Work at M.I.T. was supported by grants from the National Science Foundation (DMR-92-14853) and the Air Force Office of Scientific Research (AFOSR 91-0078).

References and Notes

(1) Bates, F. S.; Fredickson, G. H. *Ann. Rev. Phys. Chem.* **1990**, *41*, 525.
(2) Almdal, K.; Koppi, K. A.; Bates, F. S. *Macromolecules* **1992**, *25*, 1743.
(3) Harkless, C. R.; Singh, M. A.; Nagler, S. E.; Stephenson, G. B.; Jordan-Sweet, J. L. *Phys. Rev. Lett.* **1990**, *64*, 2285.
(4) Hashimoto, T.; Kowsaka, K.; Shibayama, M.; Suehiro, S. *Macromolecules* **1986**, *19*, 750.
(5) Hashimoto, T.; Kowsaka, K.; Shibayama, M.; Suehiro, S. *Macromolecules* **1986**, *19*, 754.
(6) Oono, Y.; Bahiana, M. *Phys. Rev. Lett.* **1988**, *61*, 1109.
(7) Bates, F. S. *Science* **1991**, *251*, 898.
(8) Almdal, K.; Rosedale, J. H.; Bates, F. S.; Wignall, G. D.; Fredrickson, G. H. *Phys. Rev. Lett.* **1990**, *65*, 1112.
(9) Hadziioannou, G.; Skoulios, A. *Macromolecules* **1982**, *15*, 258.
(10) Sadron, C.; Gallot, B. *Makromol. Chem.* **1973**, *164*, 301.
(11) Gallot, B. *Adv. Polym. Sci.* **1978**, *29*, 87.
(12) Shibayama, M.; Hashimoto, T.; Hasegawa, H.; Kawai, H. *Macromolecules* **1983**, *16*, 1427.
(13) Shibayama, M.; Hashimoto, T.; Kawai, H. *Macromolecules* **1983**, *16*, 1434.
(14) Shibayama, M.; Hashimoto, T.; Kawai, H. *Macromolecules* **1983**, *16*, 6.
(15) Sakurai, S.; Hashimoto, T.; Fetters, L. J. *Polym. Prepr. Jpn., Soc. Polym. Sci. Jpn.* **1991**, *40* (3), 770.
(16) Cohen, R. E.; Bates, F. S. *J. Polym. Sci. Polym. Phys. Ed.* **1980**, *18*, 2143.
(17) Thomas, E. L.; Alward, D. B.; Kinning, D. J.; Martin, D. C.; Handlin, D. L.; Fetters, L. J. *Macromolecules* **1986**, *19*, 2197.
(18) Sakurai, S.; Momii, T.; Taie, K.; Shibayama, M.; Nomura, S.; Hashimoto, T. *Macromolecules* **1993**, *26*, 485.
(19) Sakurai, S.; Hasegawa, H.; Hashimoto, T. *Polym. Prepr. Jpn., Soc. Polym. Sci. Jpn.* **1990**, *39* (3), 387.
(20) Sakurai, S.; Kawada, H.; Hashimoto, T.; Fetters, L. J. *Proc. Jpn. Acad.* **1993**, *B69*, 13.
(21) Koberstein, J. T.; Russell, T. P.; Walsh, D. J.; Pottick, L. *Macromolecules* **1990**, *23*, 877.
(22) Gruner, S. M.; Milch, J. R.; Reynolds, G. T. *Rev. Sci. Instrum.* **1982**, *53*, 1770.
(23) Tate, M. W.; Eikenberry, E. F.; Gruner, S. M. In preparation.
(24) Hasegawa, H.; Tanaka, H.; Yamasahi, K.; Hashimoto, T. *Macromolecules* **1987**, *20*, 1651.
(25) Herman, D. S.; Kinning, D. J.; Thomas, E. L.; Fetters, L. J. *Macromolecules* **1987**, *20*, 2940.
(26) Brandrup, J., Immergut, E. H., Eds. *Polymer Handbook*, 3rd ed.; Wiley-Interscience: New York, 1989; p VII/2.
(27) Brandrup, J., Immergut, E. H., Eds. *Polymer Handbook*, 3rd ed.; Wiley-Interscience: New York, 1989; p VII/15.
(28) Gotro, J. T.; Graessley, W. W. *Macromolecules* **1984**, *17*, 2767.
(29) Mays, J. W.; Hadjichristidis, N.; Fetters, L. J.; Linder, J. W. To be published.
(30) Gido, S. P.; Thomas, E. L. Submitted to *Macromolecules*.
(31) Thomas, E. L.; Anderson, D. M.; Henkee, C. S.; Hoffman, D. *Nature* **1988**, *334*, 598.
(32) Disko, M. M.; Liang, K. S.; Behal, S. K.; Roe, R. J.; Jeon, K. J. *Macromolecules* **1993**, *26*, 2983.
(33) Spontak, R. J.; Smith, S. D.; Ashraf, A. *Macromolecules* **1993**, *26*, 956.
(34) Hamley, I. W.; Koppi, K. A.; Rosedale, J. H.; Bates, F. S. To appear in *Macromolecules*.
(35) Wignall, G. D.; Ballard, D. G. H.; Schelten, J. *Eur. Polym. J.* **1974**, *10*, 861.
(36) Boothroyd, A.; Renee, A.; Wignall, G. D. To appear in *J. Chem. Phys.*
(37) Balsara, N. P.; Fetters, L. J.; Graessley, W. W.; Hadjichristidis, N.; Han, C. C.; Krishnamoorti, C.; Lohse, D. J.; Schulz, D.; Sissano, J. A. In preparation.
(38) Richardson, M. J.; Savill, N. G. *Polymer* **1977**, *18*, 3.